

## Dual Nature of Improper Ferroelectricity in a Magnetoelectric Multiferroic

S. Picozzi,<sup>1</sup> K. Yamauchi,<sup>1</sup> B. Sanyal,<sup>2</sup> I. A. Sergienko,<sup>3,4</sup> and E. Dagotto<sup>3,4</sup>

<sup>1</sup>Consiglio Nazionale delle Ricerche–Istituto Nazionale di Fisica della Materia (CNR-INFM), CASTI Regional Laboratory, 67010 L'Aquila, Italy

<sup>2</sup>Theoretical Magnetism Group, Department of Physics, Uppsala University, Box-530, SE-75121, Uppsala, Sweden

<sup>3</sup>Materials Science & Technology Division, Oak Ridge National Laboratory, Oak Ridge, Tennessee 37831, USA

<sup>4</sup>Department of Physics & Astronomy, The University of Tennessee, Knoxville, Tennessee 37996, USA

(Received 8 May 2007; published 26 November 2007)

Using first-principles calculations, we study the microscopic origin of ferroelectricity (FE) induced by magnetic order in the orthorhombic  $\text{HoMnO}_3$ . We obtain the largest ferroelectric polarization observed in the whole class of improper magnetic ferroelectrics to date. We find that the two proposed mechanisms for FE in multiferroics, lattice and electronic based, are simultaneously active in this compound: a large portion of the ferroelectric polarization arises due to quantum-mechanical effects of electron orbital polarization, in addition to the conventional polar atomic displacements. An interesting mechanism for switching the magnetoelectric domains by an electric field via a  $180^\circ$  coherent rotation of Mn spins is also proposed.

DOI: 10.1103/PhysRevLett.99.227201

PACS numbers: 75.80.+q, 75.47.Lx, 75.50.Ee, 77.80.–e

Magnetolectric materials owing their improper ferroelectric (FE) order to symmetry-breaking magnetic structures have drawn enormous recent interest [1–3]. In order to explain the microscopic origin of their electric polarization ( $P$ ), two basic mechanisms have been proposed in model studies. According to one of them, magnetic ordering results in the hybridization of electronic orbitals producing a polar charge distribution [4,5]. The other, more conventional approach, views the displacements of ions from their centrosymmetric positions (CSP) as the primary source of  $P$  [6–8]. Extensive experimental studies have not been able to distinguish between the two possibilities, due to very small values of  $P$  found in this class of multiferroics ( $P < 0.1 \mu\text{C}/\text{cm}^2$  in  $\text{TbMnO}_3$  and  $\text{TbMn}_2\text{O}_5$  [1,2]). In a quest for higher  $P$ , a recent model Hamiltonian study [8] concentrated on the collinear antiferromagnetic- $E$  (AFM- $E$ ) spin configuration, where ferromagnetic zigzag spin chains in the  $\text{MnO}_2$  planes are antiferromagnetically coupled with respect to both adjacent in-plane chains [see Fig. 1(a)] and out-of-plane stacked chains, as found in orthorhombic  $\text{HoMnO}_3$  [9]. The predicted polarization  $P = 0.5\text{--}12 \mu\text{C}/\text{cm}^2$  was much higher than in other improper magnetic ferroelectrics. However, pyroelectric current measurements on bulk polycrystalline samples revealed ferroelectricity in  $\text{HoMnO}_3$  with  $P < 2 \text{nC}/\text{cm}^2$  [10].

First-principles calculations appear to be well suited to address the two issues discussed above: (1) they can reveal the dominant mechanism of improper FE  $P$  in magnetically ordered compounds, since the electronic structure and lattice distortions can be treated simultaneously, and (2) they can estimate the value of  $P$ , which is currently highly debated. We performed simulations based on the generalized gradient approximation (GGA) [11] to density-functional theory (DFT) using the Vienna *Ab initio*

Simulation Package (VASP) [12] and the projector-augmented-wave pseudopotentials. Ho  $4f$  electrons were assumed as frozen in the core. The plane wave energy cutoff was set to 500 (400) eV for the collinear [noncollinear (NC)] calculations. The Brillouin zone sampling was performed using the  $3 \times 4 \times 6$  shell. The GGA +  $U$  [13] calculations within Dudarev's approach [14] were performed by applying a Hubbard-like potential for Mn  $d$  states. Since the  $U$  value is not known from photoemission experiments or constrained-DFT calculations for ortho- $\text{HoMnO}_3$ , we varied  $U$  from 0 to 8 eV and, accordingly, we chose  $J = 0.15U$ . The Berry phase approach [15,16] was used to calculate  $P$ , integrating over six  $\mathbf{k}$ -point strings parallel to the  $c$  axis, each string containing 6  $\mathbf{k}$  points. NC calculations were performed according to Ref. [17]. Spin-

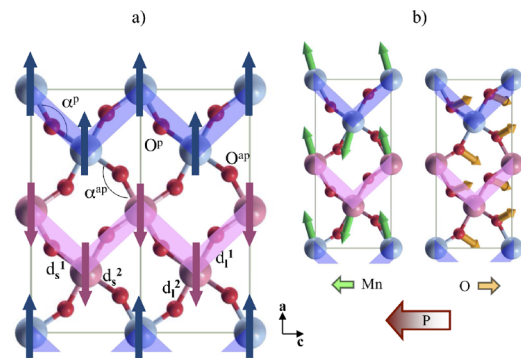


FIG. 1 (color online). (a) In-plane arrangement of Mn and O atoms. Arrows denote the direction of spins and AFM-coupled zigzag spin chains are highlighted by shaded areas. Structural parameters reported in Table I are shown. (b) Arrows show the directions of the ionic displacements for Mn (left) and O (right) in AFM- $E$ . The thick arrows at the bottom show the direction of the resulting displacements of Mn and O sublattices and  $\mathbf{P}$ .

orbit coupling (SOC) was neglected. Experimental lattice constants [18] for orthorhombic  $\text{HoMnO}_3$  were used (space group  $Pnma$ ,  $a = 5.835 \text{ \AA}$ ,  $b = 7.361 \text{ \AA}$ , and  $c = 5.257 \text{ \AA}$ ) and, starting from experimental atomic positions, we then performed atomic relaxations with Hellman-Feynman forces  $< 0.01 \text{ eV/\AA}$ .

Because of the small size of the Ho ionic radius,  $\text{HoMnO}_3$  shows [18] a highly distorted perovskite structure with the Mn-O-Mn  $ac$ -plane angle  $\alpha_0 \approx 144^\circ$ . The AFM- $E$  spin alignment is stabilized due to this strong distortion of the perovskite structure, as suggested by previous model [19,20] and first-principles [21] reports. With the optimized atomic positions obtained after imposing the spin order, we calculated  $P$  using the point charge model (PCM) with nominal charges (i.e.,  $-2e$  for O and  $+3e$  for Ho and Mn). The calculated  $P_{\text{PCM}}$  is shown in Fig. 2(b) vs the Hubbard parameter  $U$ ,  $P_{\text{PCM}}(U)$  being a decreasing function. This is consistent with the general ideas of the model calculations [8], where  $P$  appears due to the difference ( $\alpha_p - \alpha_{\text{ap}}$ ) between the Mn-O-Mn angles corresponding to the bonds with parallel ( $\alpha_p$ ) and antiparallel ( $\alpha_{\text{ap}}$ ) spins, as a consequence of the Hund's coupling and virtual electronic hopping. Since  $U$  characterizes the energy penalty paid for adding an additional electron on a Mn site, increasing  $U$  makes the virtual electron hopping less favorable, which in turn reduces  $\alpha_p - \alpha_{\text{ap}}$  and, ultimately,  $P$ . Nevertheless, as shown in Fig. 2, the effect of even a very large  $U = 8 \text{ eV}$  is to decrease  $P$  by less than half an order of magnitude. As the value of  $U$  for  $\text{HoMnO}_3$  is not known from experiments, we will resort to a parameter-free DF treatment with  $U = 0$  from now onwards, noting that the calculated quantities should be trusted only with respect to their orders of magnitude.

A close look at the geometrically optimized structure in the AFM- $E$  phase reveals complicated displacements [Fig. 1(b)]. The Mn (in-plane O) atoms displace by  $0.04 \text{ \AA}$  ( $0.02 \text{ \AA}$ ) with respect to the initial  $Pnma$  structure, with the displacement  $a$  and  $b$  components compensating

each other and the  $c$  components adding up to a net displacement of  $0.01 \text{ \AA}$  per Mn (O) atom along the negative (positive)  $c$  direction. Taking into account relatively smaller  $c$ -axis displacements of interplane O and Ho atoms, we obtain  $P_{\text{PCM}} = 2.1 \mu\text{C}/\text{cm}^2$ . Therefore, our calculations with no fitting parameters independently confirm the large  $P$  obtained in the previous model [8]. In this regard, we hope that the experimentally attained  $P$  [10] could be improved substantially as it was accomplished for another promising multiferroic  $\text{BiFeO}_3$  [22]. In parallel, the role of Ho  $4f$  spins in the microscopic origin of  $P$  (clearly relevant in experiments [10] and neglected here) should be addressed in future theoretical studies.

To have a better understanding of the structural distortions caused by the magnetic order, we also optimize the structural parameters for the paraelectric (PE) AFM- $A$  (all spins in the  $ac$  plane parallel) and AFM- $G$  (all neighboring spins antiparallel) phases and compare them to AFM- $E$  (see Table I). In agreement with the above discussion,  $\alpha_p$  for AFM- $A$  is larger than  $\alpha_{\text{ap}}$  for AFM- $G$  in the whole  $U$  range [see Fig. 2(a)]. However, when both types of angles ( $\alpha_p$  and  $\alpha_{\text{ap}}$ ) are present in the AFM- $E$  phase, this difference is even more pronounced, which explains the relatively high  $P$ .

The AFM- $E$  phase shows two different kinds of AFM domains [8],  $E_1$  and  $E_2$  (left and right insets of Fig. 3(a), respectively), expected to show opposite polarization,  $-P_c$  and  $P_c$ . In our calculational unit cell,  $E_1$  and  $E_2$  differ in the orientation of half of the spins (see gray highlighted regions in the central inset). Here, we consider a FE-AFM switching path from  $-P_c$  ( $E_1$ ) to  $P_c$  ( $E_2$ ) via a progressive rotation of the central spins. According to the basic displacementlike mechanism for  $P$ , we expect  $P$  to switch from negative (in  $E_1$ ) to positive (in  $E_2$ ) and to vanish when the relative orientation of the central spins with respect to the fixed spins is close to  $90^\circ$ . The  $90^\circ$  spin configuration, denoted as  $\perp$  [central inset of Fig. 3(a)], is an example of a spiral magnetic structure similar to that in  $\text{TbMnO}_3$ , but commensurate with the modulation vector  $\mathbf{k} = (1/2, 0, 0)$ , and which should be FE with  $P_\perp$  along the  $c$  axis [4,6,23,24]. Based on the macroscopic symmetry considerations [25], the polarization vector  $\mathbf{P}$  can be expressed as

$$P_c = \chi_z(c_{xz} \sin \phi - c_0 \cos \phi), \quad P_a = c'_{xz} \chi_x \sin \phi, \quad P_b = 0, \quad (1)$$

TABLE I. Relevant structural parameters for the AFM- $A$ ,  $G$ , and  $E$  spin configurations: Mn-O-Mn angle (in degrees) for parallel ( $\alpha_p$ ) and antiparallel ( $\alpha_{\text{ap}}$ ) Mn spins, large ( $d_l^1$  and  $d_l^2$ ) and small ( $d_s^1$  and  $d_s^2$ ) Mn-O bond lengths (in  $\text{\AA}$ ).

|          | $\alpha_p$ | $\alpha_{\text{ap}}$ | $d_l^1$ | $d_l^2$ | $d_s^1$ | $d_s^2$ |
|----------|------------|----------------------|---------|---------|---------|---------|
| AFM- $A$ | 143.8      | ...                  | 2.20    | 2.20    | 1.93    | 1.93    |
| AFM- $G$ | ...        | 142.8                | 2.24    | 2.24    | 1.90    | 1.90    |
| AFM- $E$ | 145.3      | 141.9                | 2.25    | 2.18    | 1.92    | 1.92    |

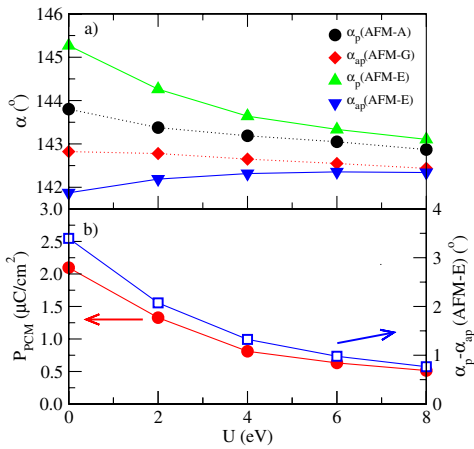


FIG. 2 (color online). (a) Mn-O-Mn angles (in degrees),  $\alpha_p$  and  $\alpha_{\text{ap}}$ , vs  $U$ . (b)  $P_{\text{PCM}}$  and  $\alpha_p - \alpha_{\text{ap}}$  vs  $U$  in AFM- $E$ .

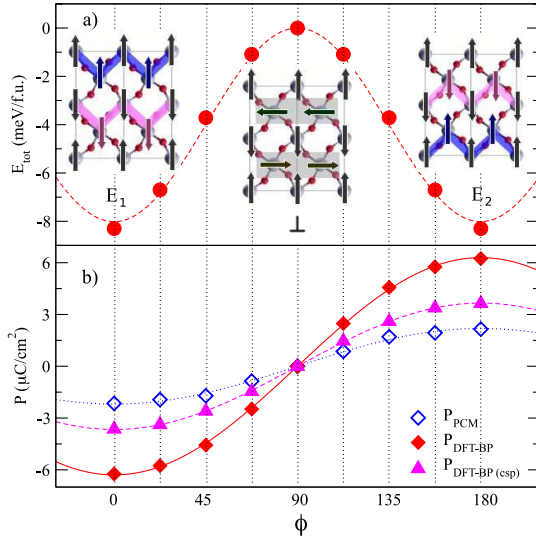


FIG. 3 (color online). (a) TE vs the orientation of the central spins (see gray highlighted regions in the central  $\perp$  spin-configuration) with respect to the spin of the Mn in the origin. (b)  $P$  calculated via PCM [empty (blue) diamonds], via DFT-BP [filled (red) diamonds] and via DFT-BP for CSP [triangles (pink); see text]. The lines are fits to  $P \propto \cos\phi$  with constant coefficients.

where  $\chi_x$  ( $\chi_z$ ) is the component of the dielectric susceptibility along the  $a$  ( $c$ ) axis and  $\phi$  is the rotation angle of the central spins. The coefficient  $c_0$  stems from nonrelativistic interactions, while  $c_{xz}$  and  $c'_{xz}$  originate from the coupling of  $P$  to the product of the  $a$  and  $c$  components of the Mn spins, which has a relativistic origin. Equations (1) lead to several important conclusions: (i) for the commensurate spiral state  $\perp$  ( $\phi = \pi/2$ ), a longitudinal component  $P_a$  of the uniform polarization is present in addition to  $P_c$ ; (ii)  $P_\perp$  is finite due to purely relativistic effects, in agreement with previous microscopic models [4,6]; (iii) since the relatively small relativistic effects such as SOC are neglected in our computations, we observe that only the  $c$  component of  $\mathbf{P}$  is finite for all  $\phi$  and  $P \propto \cos\phi$ , in excellent agreement with the numerical results in Fig. 3(b), which are discussed below. Also, in our computations  $P_\perp = 0$ , and  $\perp$  is taken as the reference PE structure with CSP.

If FE switching is to occur, as the spin rotation proceeds starting from  $E_1$ , the total energy (TE) is expected to increase up to a maximum corresponding to the PE state ( $\perp$ ), and then to decrease again until the  $E_2$  minimum is reached. Indeed, this happens when we perform the NC calculations by varying  $\phi$  between 0 and  $180^\circ$  with fully optimized atomic coordinates for each spin configuration. The calculated TE vs  $\phi$  [see Fig. 3(a)] clearly shows a double-well structure, with the depth of the well of  $\sim 8$  meV/formula unit (f.u.). Although the exact magnitude of the depth of the well can be affected by computational details and approximations, we still expect the feasibility of the magnetoelectric switching by the appli-

cation of realistic electric fields. The calculated energy barrier is, in fact, smaller than in proper FE  $\text{BaTiO}_3$  (18 meV/f.u.) and  $\text{PbTiO}_3$  (200 meV/f.u.), and multiferroic  $\text{BaMF}_4$  ( $>20$  meV/f.u.) [26]. We further remark that the AFM-FE switching path is proposed as an energetically “upper bound,” not necessarily as the path occurring in experiments during switching. In addition, as detailed below, this also constitutes an adiabatic path along which one can calculate and reverse  $P$ , so the overall picture appears consistent and self-contained.

The evaluation of  $P$  deserves a careful discussion, since it leads to an intriguing outcome. In Fig. 3(b), we report  $P$  evaluated by the PCM and Berry-phase (BP) approaches within the density-functional-theory (DFT-BP) along the previously mentioned switching path. [27,28] The marked disagreement between the PCM and DFT-BP approaches suggests that quantum electronic effects are at play in determining the final  $P$ , similar to the conventional FEs [29]. To investigate the purely electronic effects, we calculate  $P$  considering the atomic positions of the  $\perp$  structure and artificially switching the spin configuration, without relaxing the lattice degrees of freedom. In this case, because of structural centrosymmetry, there is no contribution from atomic displacements. However, the calculated BP polarization is found to be up to  $3.5 \mu\text{C}/\text{cm}^2$  [see triangles in Fig. 3(b)]. This large contribution arises solely from the electronic contribution due to symmetry breaking by the AFM- $E$  ordering.

The quantum effects can be quantified further by considering the deviations of the Born effective charges (BEC) from their nominal valencies. In the  $\perp$  case, when each O is coordinated to two Mn with perpendicular spins, we obtain for the 33 component of the BEC tensor  $Z_\perp^*$  (Mn) =  $3.9e$  and  $Z_\perp^*$  (O) =  $-3.1e$ . Along the AFM-FE switching path, the O ions  $O^p$  and  $O^{\text{ap}}$  become increasingly different

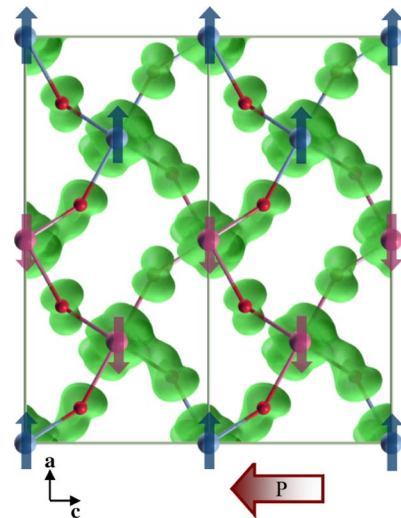


FIG. 4 (color online). The  $ac$ -plane charge density isosurface plot in the energy range  $[-0.8:0]$  eV (top of valence band set as zero of the energy scale) for relaxed positions in AFM  $E_1$ .

and acquire different BEC due to the orientation of the Mn spins to which they are bonded. In the extreme points corresponding to  $E_1$  and  $E_2$ , we obtain:  $Z^*(\text{Mn}) = 3.8e$ ,  $Z^*(\text{O}^p) = -2.6e$ , and  $Z^*(\text{O}^{\text{ap}}) = -3.5e$ . In both  $\perp$  and  $E$ -type spin arrangements, the BEC are not extremely different from their nominal valence, consistent with a rather ionic nature of the chemical bonds. The two different kinds of O ions are responsible for ferroelectricity in the case of CSP, where the displacement mechanism is switched off. However, upon allowing atomic relaxation, all the atoms (including displaced Mn) contribute to the final FE  $P$ . The inequivalence of  $\text{O}^p$  and  $\text{O}^{\text{ap}}$  is further confirmed by the charge density plot, corresponding to the energy range of hybridized Mn  $e_g$  and O  $p$  orbitals located just below the valence band maximum (see Fig. 4). In addition to the expected checkerboardlike orbital ordering [9,19], Fig. 4 clearly demonstrates the strong asymmetry in the charge distribution between the two kinds of O ions. Moreover, focusing on  $\text{O}^{\text{ap}}$ , the charge seems to favor the short Mn-O bond compared to the long bond. This suggests that the polar charge distribution is due to a delicate combination of the Jahn-Teller effect and symmetry-breaking magnetic ordering.

In summary, our first-principles results show that, in the AFM- $E$ -type  $\text{HoMnO}_3$ , the symmetry-induced inequivalence of the in-plane Mn-O-Mn configurations for parallel and antiparallel spins is an efficient mechanism in driving a considerable ferroelectric polarization. The calculated polarization of the AFM- $E$  phase,  $P \approx 6 \mu\text{C}/\text{cm}^2$ , is consistent with previous theoretical estimates [8]. In addition to the displacement mechanism, we find a larger but comparable contribution arising from a purely electronic quantum effect of orbital polarization. The finite ferroelectric polarization, even with a centrosymmetric atomic arrangement, is an unambiguous indication of a magnetism-induced electronic mechanism at play. Also, a magneto-electric domain switching path is proposed, in which the reversal of polarity of the applied electric field induces a  $180^\circ$  flip of selected spins. Although we focused on the case of  $\text{HoMnO}_3$  as an example, we believe our results concerning the dual nature of ferroelectricity as arising from a symmetry breaking induced by the magnetic order should have a wider validity for improper magnetic ferroelectrics. Our findings suggest that the interpretation of experiments, as well as model calculations, should take into account *both* the lattice and electronic mechanisms of improper ferroelectricity in multiferroics.

Computational support from Barcelona Supercomputing Center and Swedish National Infrastructure for Computing (SNIC) is acknowledged. Research at ORNL is sponsored by the Division of Materials Sciences and Engineering, Office of Basic Energy Sciences, U.S. Department of Energy, under Contract No. DE-AC05-00OR22725 with Oak Ridge National Laboratory, managed and operated by UT-Battelle, LLC. I. S. and E. D. are supported in part by

NSF Grant No. DMR-0706020.

- 
- [1] T. Kimura, T. Goto, H. Shintani, K. Ishizaka, T. Arima, and Y. Tokura, *Nature (London)* **426**, 55 (2003).
  - [2] N. Hur, S. Park, P. A. Sharma, J. S. Ahn, S. Guha, and S. W. Cheong, *Nature (London)* **429**, 392 (2004).
  - [3] S. W. Cheong and M. Mostovoy, *Nature Mater.* **6**, 13 (2007).
  - [4] H. Katsura *et al.*, *Phys. Rev. Lett.* **95**, 057205 (2005).
  - [5] C. Jia, S. Onoda, N. Nagaosa, and J. H. Han, *Phys. Rev. B* **74**, 224444 (2006).
  - [6] I. A. Sergienko and E. Dagotto, *Phys. Rev. B* **73**, 094434 (2006).
  - [7] N. Aliouane *et al.*, *Phys. Rev. B* **73**, 020102(R) (2006).
  - [8] I. A. Sergienko, C. Şen, and E. Dagotto, *Phys. Rev. Lett.* **97**, 227204 (2006).
  - [9] A. Muñoz *et al.*, *Inorg. Chem.* **40**, 1020 (2001).
  - [10] B. Lorenz, Y. Q. Wang, and C. W. Chu, *Phys. Rev. B* **76**, 104405 (2007); B. Lorenz *et al.*, *Phys. Rev. B* **70**, 212412 (2004).
  - [11] J. P. Perdew *et al.*, *Phys. Rev. Lett.* **77**, 3865 (1996).
  - [12] G. Kresse and J. Furthmüller, *Phys. Rev. B* **54**, 11169 (1996).
  - [13] V. I. Anisimov, F. Aryasetiawan, and A. I. Lichtenstein, *J. Phys. Condens. Matter* **9**, 767 (1997).
  - [14] S. L. Dudarev *et al.*, *Phys. Rev. B* **57**, 1505 (1998).
  - [15] R. D. King-Smith and D. Vanderbilt, *Phys. Rev. B* **47**, 1651 (1993).
  - [16] R. Resta, *Rev. Mod. Phys.* **66**, 899 (1994).
  - [17] D. Hobbs, G. Kresse, and J. Hafner, *Phys. Rev. B* **62**, 11556 (2000).
  - [18] A. J. Alonso, M. J. Martínez-Lope, M. T. Casais, and M. T. Fernández-Díaz, *Inorg. Chem.* **39**, 917 (2000).
  - [19] T. Hotta, M. Moraghebi, A. Feiguin, A. Moreo, S. Yunoki, and E. Dagotto, *Phys. Rev. Lett.* **90**, 247203 (2003).
  - [20] T. Kimura *et al.*, *Phys. Rev. B* **68**, 060403(R) (2003).
  - [21] S. Picozzi, K. Yamauchi, G. Bihlmayer, and S. Blügel, *Phys. Rev. B* **74**, 094402 (2006).
  - [22] J. B. Neaton *et al.*, *Phys. Rev. B* **71**, 014113 (2005).
  - [23] M. Mostovoy, *Phys. Rev. Lett.* **96**, 067601 (2006).
  - [24] M. Kenzelmann *et al.*, *Phys. Rev. Lett.* **95**, 087206 (2005).
  - [25] See EPAPS Document No. E-PRLTAO-99-004748 for an explicit derivation of selected results of the Landau theory of phase transitions as applied to the antiferromagnetic  $E$ -type ordering and its coupling to ferroelectricity. For more information on EPAPS, see <http://www.aip.org/pubservs/epaps.html>.
  - [26] C. Ederer and N. A. Spaldin, *Phys. Rev. B* **74**, 024102 (2006).
  - [27] Even without  $U$ , the density of states shows an insulating character along the whole spin-rotating switching path.
  - [28] When estimating  $P$  within the BP approach by varying  $U$  in the case of optimized positions,  $P_{\text{DFT-BP}}$  shows a decreasing behavior with  $U$ , similar to the ionic-only contribution (cf. Fig. 2). However,  $P$  remains of the order of few  $\mu\text{C}/\text{cm}^2$  (i.e.,  $P \sim 4 \mu\text{C}/\text{cm}^2$  for  $U = 8 \text{ eV}$ ).
  - [29] W. Zhong, R. D. King-Smith, and D. Vanderbilt, *Phys. Rev. Lett.* **72**, 3618 (1994).